

Article

Development of a New Battery Management System with an Independent Balance Module for Electrical Motorcycles

Jeng-Chyan Muti Lin

Electrical Engineering Department, National Chinyi University of Technology, No. 57, Sec. 2, Zhongshan Rd., Taiping Dist., Taichung 41170, Taiwan; mutilin@ncut.edu.tw; Tel.: +866-9-5333-8187; Fax: +866-4-2392-4505

Received: 3 July 2017; Accepted: 26 August 2017; Published: 29 August 2017

Abstract: Conventional balance modules are integrated with the battery management system (BMS) and occupy a large area of the BMS system. In addition large balance currents generate high heating rates and require heat dissipation mechanisms. This study proposes an independent structure for the balance module. Specifically the balance module is removed from of the BMS and is integrated with an off board charger. A new BMS structure is therefore created with a simplified BMS inside the battery module and the heat dissipation requirement for the balance module could be easily met on the charger side. The design, fabrication and test of this new type of BMS on a 72 V heavy electric motorcycle application is detailed in the current work. The new BMS reduces the space and weight required for the BMS in the e-motorcycle. Complexity in the battery module or on the EV side is significantly reduced. The heat dissipation problem associated with the large balance current is also resolved by moving the balance module to the charger end.

Keywords: battery management system (BMS); active balance; e-motorcycle

1. Introduction

Discrepancies in cell internal resistance and differences in cell capacity are common among cells connected in series. Cell inconsistencies might lead to cell overcharging and overdischarging. Without an effective balancing mechanism in the battery management system (BMS), the lifetime of battery modules could be prematurely shortened and this could lead to catastrophic disasters [1,2]. The BMS is therefore imperative for active or passive balance circuits to overcome the inconsistency problems among serially connected cells.

Passive balancing methods and active balancing methods are two frequently adopted types of balance method. In passive methods, low power resistors are used to shunt charging currents to overcome the inconsistency among cells in series [3–5]. Due to the severe limitation of power ratings, passive methods are slow and inefficient. If fast balance is needed, high resistors with high heat generation are required with passive methods. High heat generation in the BMS necessitates costly heat dissipation mechanisms within the BMS. With passive methods, if the inconsistency level is high among cells, overcharging is unavoidable in practice. Overcharging has a negative effect on cell lifespan, so if possible, any level of overcharging should be avoided. Overall passive methods have low efficiency and are not suitable for large storage capacity applications.

Active balance methods equalize inconsistencies among cells in series by moving electrical energy from higher state of charge (SOC) cells to lower SOC cells. References [5–8] used small capacitors and inductors as storage medium to actively transfer electrons between neighboring cells. However, usually the capacitors or inductors adopted in active balance schemes are small and the resulting balance currents are small. Texas Instruments Inc. (Dallas, TX, USA) developed a PowerPump™

balance IC which used two MOSFETs and capacitors to pump charges between neighboring cells to equalize cell inconsistencies with a balance current of less than 200 mA [9].

By moving electrons between cells with high efficiency active balance methods are intrinsically more efficient than passive balance methods. However, when electrical energy is transferred between cells that are not in the immediate neighborhood, active methods could be inefficient. Existing active balance methods work best for small numbers of cells in series. One more drawback of active methods is the frequency of exchanging electrical energy is too high in most active methods. High frequency of charging or discharging in lithium ion cells could accelerate the cell degradation rate. If the active balance scheme is not well planned, over discharging might result from cells with high levels of inconsistency.

Lin [10] adopted a global type active balance method with a large balance current to improve the shortcomings of local type active balance methods. Figure 1 is a schematic of a globally active balance circuit. In Figure 1, the power source of the balance block is the 72 V charger and the balance block is regulated by a forward converter with a 5 V output. The balance current can be large if the power rating of the forward converter is large too. A forward converter module FEWS-6005.5B30 made by Danube (Kaohsiung, Taiwan) [11] is adopted in the current study.

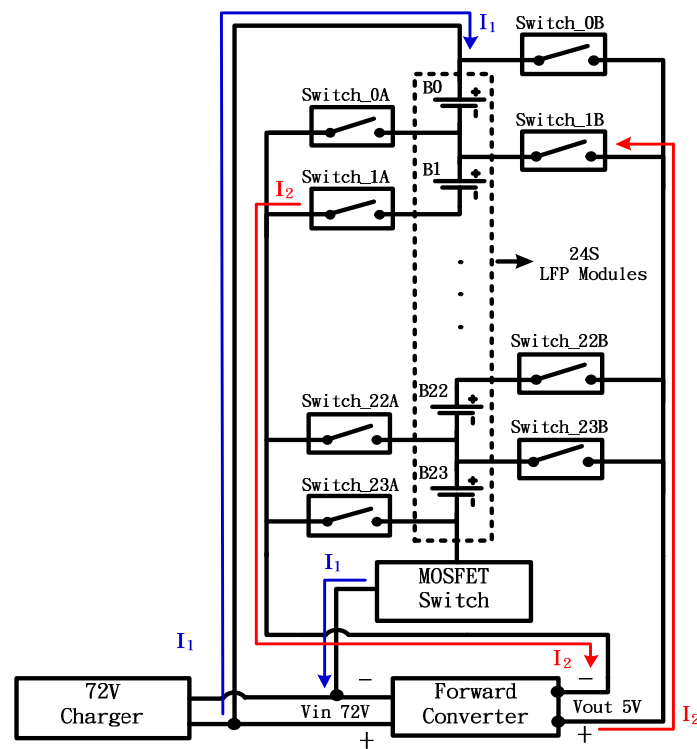


Figure 1. Globally active balance circuit.

Figure 2 is the circuit of the adopted forward converter. In the forward converter circuit of Figure 2, a transformer is used for voltage reduction and circuit isolation. This converter balances weak cells with a 6 A balance current with rated 85% efficiency. In Figure 1, any weak cell is selected by two opto coupling type relays in the relay matrix. Since any cell in Figure 1 can be selected to be balanced by the forward converter, this balance method is therefore a global type. This global type balance circuit selects the weak cell and transfers external energy until equalization among cells is reached. The MOSFET switch in Figure 1 is used to cut off charging process when any cell is overcharged. Six NXP BUL956R1-100E N-MOSFETs (NXP Semiconductors N.V., Eindhoven, The Netherlands) [12] in parallel are adopted along with a RCD snubber to suppress voltage spikes while switching on and off. The schematic of the MOSFET switch is shown in Figure 3. The developed global type balance

circuit has the advantages of larger balance current, shorter balance time, and higher efficiency. Table 1 compares the characteristics of the various balance methods.

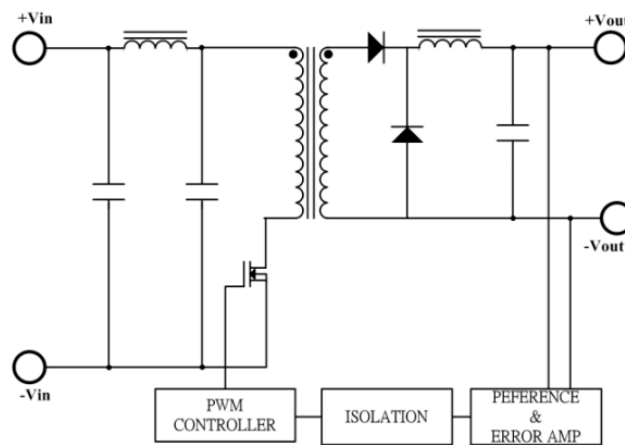


Figure 2. Schematic circuit of the forward converter [11].

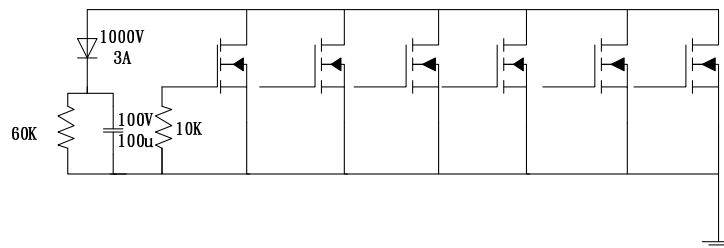


Figure 3. Schematic of the MOSFET switch in Figure 1.

Conventionally, balance circuits are built inside the BMS. However, balance circuits with large balance currents will occupy about 50% of the BMS PCB area and demand active heat dissipation. From in-house experience and commercial case observation, balance modules with large balance currents inside the BMS require roughly the same amounts of electronic components to construct as the rest of the BMS circuits. Therefore, the weight and space of the BMS PCB without balance module is roughly 50% of the original BMS PCB with balance module in the same PCB. In order to simplify the BMS inside the battery module, this study redesigns the structure of the BMS by separating the balance circuit from the BMS and integrating the balance module with a charger. In the charger end, problems associated with heat dissipation, space, and complexity for the BMS with built-in balance module can be easily resolved since off board charger has no space limitation and has a built in fan for cooling. In the following method section, a two-staged charging and balancing method facilitated by a globally active balance module for the current study is explained. The new BMS is tested on an electrical motorcycle and experimental results are detailed in Section 3. Finally, conclusions are drawn in the last section.

Table 1. Comparison of various balance methods.

Balance Method	Passive Balance [3–5]	Capcitor/Inductor Based Active Balance [5–8]	Globally Active Balance [10]	Two Stage Charging and Balancing [10]
When to Balance	Charging	Charging/Discharging/Idle	Charging/Discharging/Idle	Charging/Discharging/Idle
Balance Current	200–500 mA	200–500 mA	3–10 A	3–12 A
Balance Target	High Voltage Cell	Neighboring Cells	Low Voltage Cell	Low Voltage Cell
Balance Efficiency	Low	Medium	High	High
Overcharged Possibility	Yes	Yes	Yes	No

2. Methods

In order to improve problems of space, cost and heat dissipation associated with the placement of the built-in balance module inside the BMS, this study divides a 72 V BMS into two subsystems: a 72 V main control subsystem and a 72 V balance subsystem. Figure 2 is the developed BMS. As shown in Figure 2, 72 V main control subsystem is electrically connected with the 72 V lithium iron phosphate (LFP) battery module in the vehicle. The separate 72 V balance module is integrated with the charger as indicated in Figure 4.

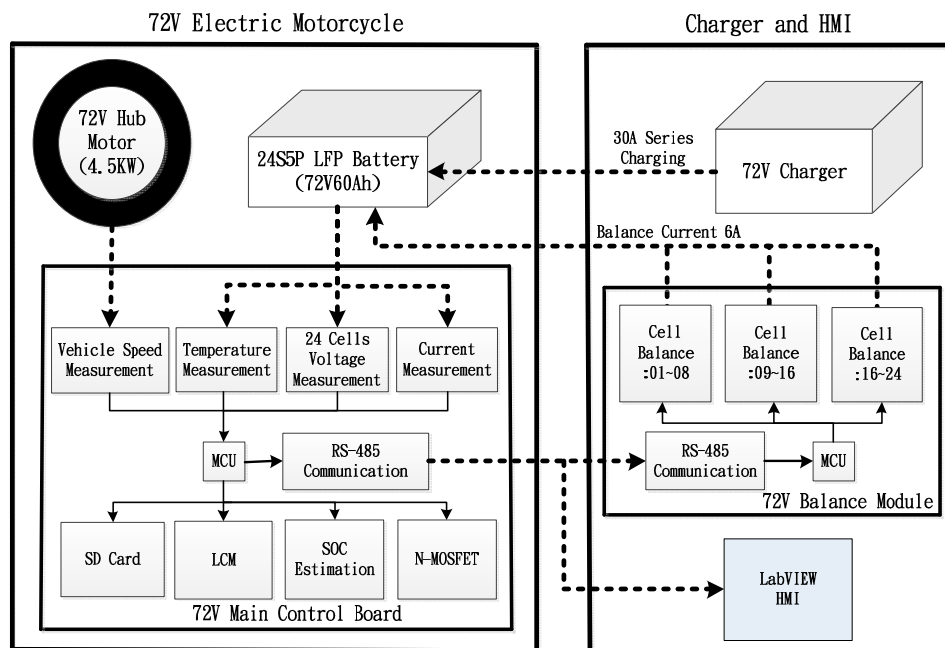


Figure 4. Proposed BMS system.

2.1. 72 V Main Control Subsystem

The main control subsystem of Figure 4 is designed to manage a 72 V/24 S LFP battery module and is based on a micro-control processor (MCU) PIC18F87K22 [13] (Microchip Technology Inc., Chandler, AZ, USA). The control subsystem measures the voltages and temperatures of the 24 LFP cells, battery module currents, and the speed of the vehicle. The measured battery parameters are shown and stored in a built-in liquid crystal module (LCM) and SD card. A two-staged charging and balancing method facilitated by a globally active balance module is implemented and is explained in details later. A hybrid SOC estimation method [10] is employed to predict remaining capacity with confidence. A protection relay consisted of N-type MOSFET is used for protection purposes. An isolated RS-485 communication system is adopted to make bilateral connection with a Human Machine Interface (HMI) computer for real-time monitoring. The prototype of the 72 V control subsystem is shown in Figure 5 with explanations of the constituent circuits inside the photo.

The control subsystem measures the cell voltages through a matrix of LT 233 opto relays (Lextex Technology Corp., Taichung, Taiwan) [14]. By selecting the right opto relay pairs, the cell voltage can be measured by connecting the cell to one analog to 12 bits digital converter (ADC) every 10 nanoseconds. The major advantage of this voltage measurement technique as shown in [15] is to preserve the high degree of accuracy of each cell voltage measurement, within 10 mV, regardless of how many numbers of cells are connected in series. The stack temperature is measured by a thermal resistance sensitive (TRS) component with negative temperature coefficient (NTC) to prevent any high temperature situation. Monitoring the stack temperature in real-time allows the control subsystem to take protection measures before heat runaway occurs.

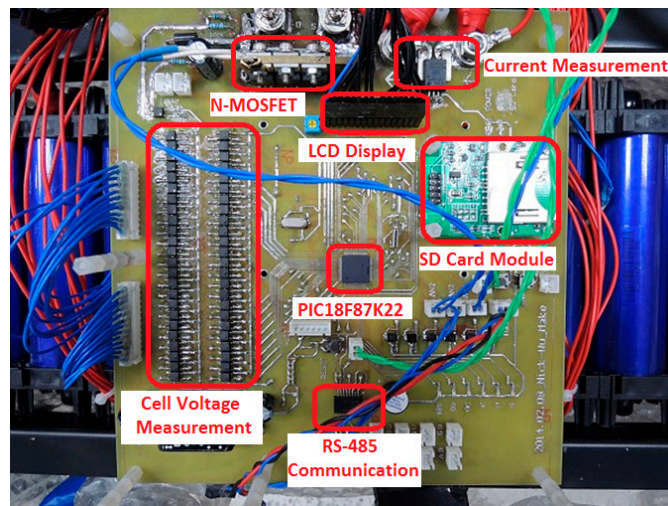


Figure 5. 72 V main control subsystem.

This investigation uses an ACS756 (Allergo Microsystems LLC, Worcester, MA, USA) [16] Hall type current sensor for measuring the real-time current. The ACS756 is low in form factor, convenient to use, and driven by a 5 V source. It can measure currents of up to 200 A. The relative error of the ACS756 is 0.3% of the full scale. Accurate measurement of the battery current is important for SOC prediction via a Coulomb counting method. Vehicle speed is measured by a WSH132 (Winson Semiconductor Corp., Hsinchu, Taiwan) Hall sensor [17] and a permanent magnet which is rotated with the vehicle wheel. When the magnet passes through the Hall sensor, the Hall sensor will generate a high or 5 V signal to the MCU of the control subsystem. The frequency of the high signals is counted and converted to speed of the vehicle accordingly.

The control subsystem measures and monitors cell voltage, cell temperature and module current. When extreme conditions occur in the battery, the control subsystem conducts warning and protection procedures. Estimation of SOC is also built into the control subsystem. In the current study a hybrid method is used for LFP SOC estimation. The hybrid method divides the battery operation zone into high, main and low SOC zones. The Coulomb counting method is employed in the main SOC zone to overcome low differentiation between cell voltage and SOC of LFP. The electrical motive force (EMF) correlation method is used in high and low SOC zones. In conjunction with a two-staged charging method, the current hybrid SOC estimation method predicts battery SOC within 5% accuracy. Battery and vehicle operation information is presented in the LCM for real-time monitoring purposes. Operation data is stored in the embedded SD card for post-analysis purposes.

When charging, the control subsystem coordinates the balance module and controls the two-staged charging process, as detailed in Figure 6, and serial charging and parallel charging stages can be completed without overcharging any cell. Communication between the control subsystem and balance module is enabled by an isolated two-way RS-485 IC (Analog Devices, Inc., Norwood, MA, USA) [18].

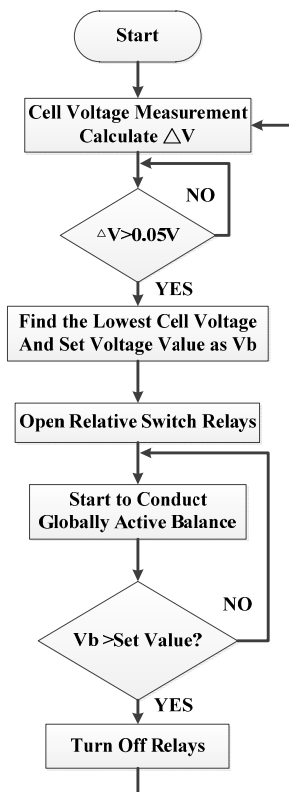


Figure 6. Two-staged charging flowchart.

2.2. 72 V Balance Subsystem

This study separates the balance function from the BMS and integrates the balance module with a charger. Integrating the balance module with a charger can save space and avoid the heat dissipation needed inside the battery module. Figure 7 is a photo of the separate balance module identifying its parts. The key of the balance module is the globally active balance circuit, which consists of a matrix of opto relays as shown in Figure 1. A 72 V battery module consists of 24 LFP cells connected in series. The balance module is electrically connected with the battery module.

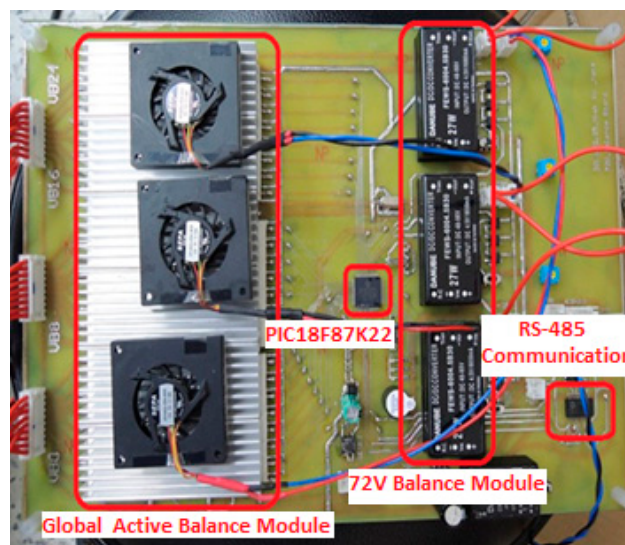


Figure 7. 72 V balance module.

Electronic relays and forward converters are keys to the balance module in Figure 1. The balance module selects the lowest voltage cell with the corresponding pair of electronic relays. Electricity converted from the charger by the forward converter is injected into the selected weak cell one at a time. One cell needs a pair of relays to select the cell. Isolated relays are required in the balance module to turn on and off the balance power for the weak cell. An isolated opto relay LT 218 from Letex Inc. (Letex Technology Corp., Taichung, Taiwan) [19] is adopted in the current study. The balance source is supplied by the 72 V charger and charger output voltage is converted to 4.5 V by a forward converter [11]. When one cell is selected by the balance module, this cell is charged by a constant voltage mode with current ranges from 4 A to 6 A by design. When the balanced cell voltage reaches the preset voltage limit of 3.65 V, the balance power is turned off immediately to avoid overcharging. In the current study a 24 S battery module is divided into three groups and each group is balanced by one forward converter. Therefore three cells are balanced simultaneously and the total balancing time is reduced.

2.3. Two Staged Charging and Balancing Logic

This investigation designs a two staged charging and balancing logic. In the first stage, the charger in Figure 1 charges the battery at I_1 of 72 V and injects I_2 at 4.5 V into the weak cell for equalization. I_2 switches among cells when balanced condition is triggered. Triggering balance conditions are set at 30 mV difference among cells in series connection. The first stage is terminated after a predetermined high voltage state is exceeded. I_1 is terminated and second stage takes control.

In the second stage, cells in series connection are charged one by one at I_2 of 4.5 V as depicted in Figure 1. Each cell is fully charged sequentially in the second stage. When all the cells in the battery module are fully charged, second stage and also the charging process are terminated. With this two staged charging and balancing logic, fully charged states are realized for each cell in the battery module. Furthermore, overcharging is avoided completely.

3. Experiments and Results

A 72 V electric heavy motorcycle as shown in Figure 8 was designed and fabricated in the current study to test the performance of the developed BMS. The current study utilizes the developed global type active balance method [10] in developing a 72 V BMS. This 72 V BMS is controlled by an 8-bit PIC18F87K22 MCU. This BMS possesses accurate measurement of cell voltages and practical estimation of battery SOC. Data acquisition circuits were built in the main control subsystem to simplify testing. The accuracy of the self-made acquisition system is thoroughly tested and compares with calibrated high accurate instruments. Accuracies of measured parameters, voltages, currents and speeds, are all within 1% of respective full scale.

The test platform in Figure 8 is composed of one complete electric motorcycle with a rear hub motor of 72 V, a 72 V/60 Ah recycled LFP battery module, the main control subsystem electrically connected with the battery module, a battery charger of 72 V, and an independent balance module in the charger end. When charging the battery module with the two staged charging method, the balance module is electrically connected to the main control system by 25 wires as balance conduits and RS-485 wire for communication between the main control subsystem and balance module. An electrically isolated RS-485 IC is adopted to avoid electromagnetic interferences.

Recycled LFP battery cells are adopted in the current study to demonstrate the unique feature of the developed balance method. The adopted LFP battery cells have a wide spread of characteristics. Cell capacity varies from 9 Ah to 12 Ah and internal resistance varies from 1.5 m Ω to 4.5 m Ω . For a 60 Ah module, six cells are connected in parallel and the average internal resistance for each module is about 0.5 m Ω . The wide variation of the LFP modules in series poses great challenges for any BMS's balance capability. This study attempts to charge each module fully without overcharging any module in series.

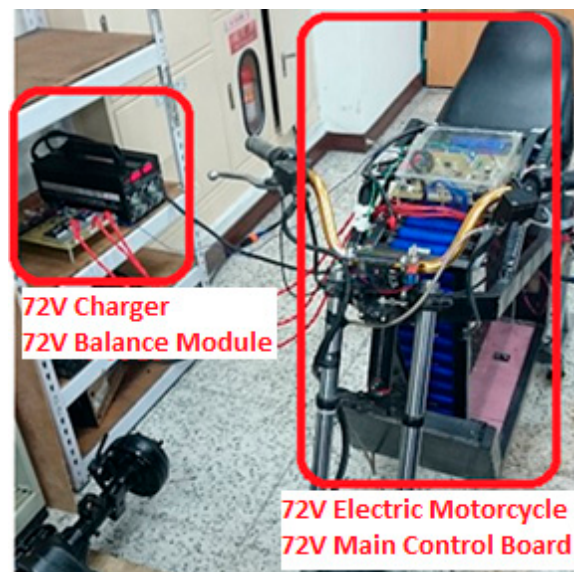


Figure 8. Charging platform with independent balance module.

3.1. Tests of a Two Stage Charging Method

Tests of the two stage charging method developed by the current study were conducted in the test platform of Figure 8. The charging process is monitored by a LabView-based HMI developed for this study. The results are presented in Figure 9, where real-time values of 24 cell voltages during the charging process are plotted versus charging time in seconds. Initially, the maximum cell voltage difference of the battery is 360 mV before charging. In the first stage, after every cell reaches a predetermined overcharged voltage, first stage charging ends and second stage charging begins. In Figure 9, twenty four peaks near 3.6 V characterize the completion of the second stage and the whole charging process. The voltage difference among the 24 cells stays smaller than 20 mV a few minutes after the whole charging process ends as indicated in Figure 9.

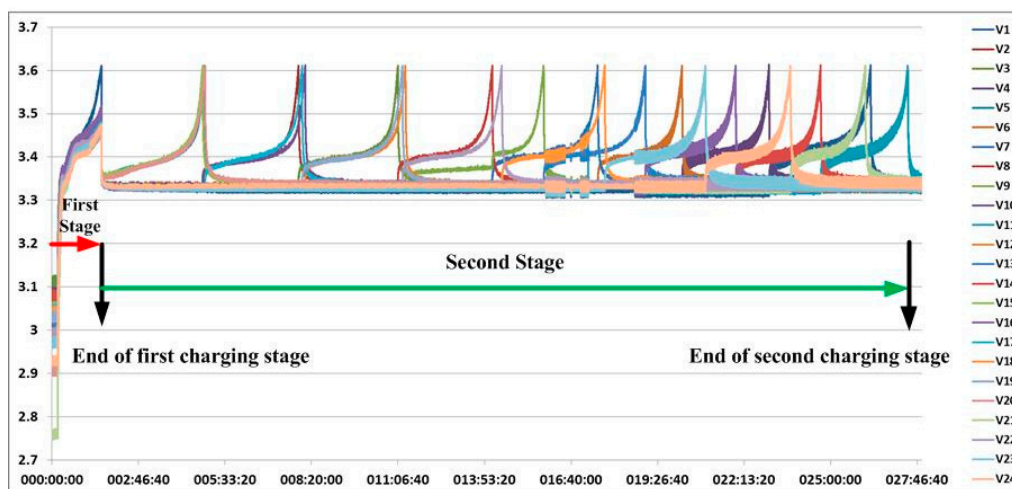


Figure 9. Results of the two-staged charging method.

3.2. Discharging Tests

The discharging tests were conducted on the 72 V heavy electrical motorcycle shown in Figure 8. Battery and vehicle operation parameters were extracted by the main control subsystem and recorded at 1 second intervals in the built-in SD card for post-processing. Figures 10–13 are the results for

a typical test drive of the e-motorcycle over a regular road in Taiwan. Figure 10 is the cell voltage discharging history. Initially the maximum cell voltage difference among the 24 cells was about 20 mV and at the end the voltage difference was more than 530 mV as shown in Figure 10.

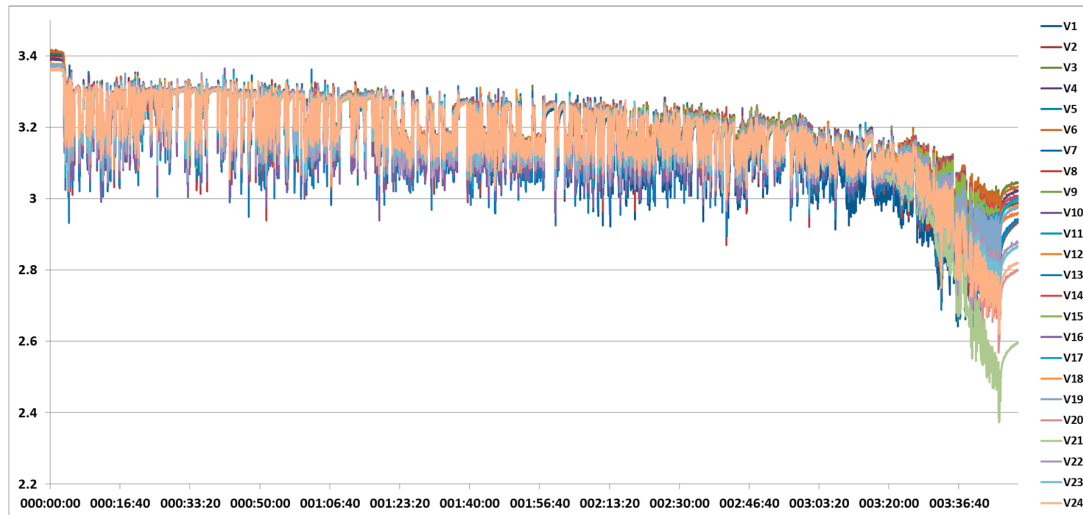


Figure 10. Discharging cell voltage histories.

Figure 11 shows the voltage and current histories for the main battery. The complete trip takes about 3 h and 47 min before undervoltage is approached. The average power consumption of the hub wheel motor is about 3.9 kW, obtained from multiplying the battery voltage and current and taking average over the complete trip. Figure 12 shows vehicle speed and accumulated mileage histories for the trip. Average speed of the trip is about 40 km/h and the total mileage of the trip was 111.2 km.

Figure 13 presents the battery voltage, accumulated mileage, and SOC histories. The initial SOC after two-staged charging is 100%. After driving or discharging for 3 h and 27 min, the SOC drops from 13.5% to 10%.

The abrupt change of SOC is implemented by the hybrid SOC estimation method adopted by the current study. Since the condition of switching from a Coulomb counting method to an EMF correlation method is met, SOC is switched according to the EMF value at that transition point. This hybrid SOC method is therefore capable of adapting to cell inconsistencies or cell aging. Calibration of the cell capacity fade is also allowed in such structure. A detailed description on the developed hybrid SOC method is under preparation for publication.

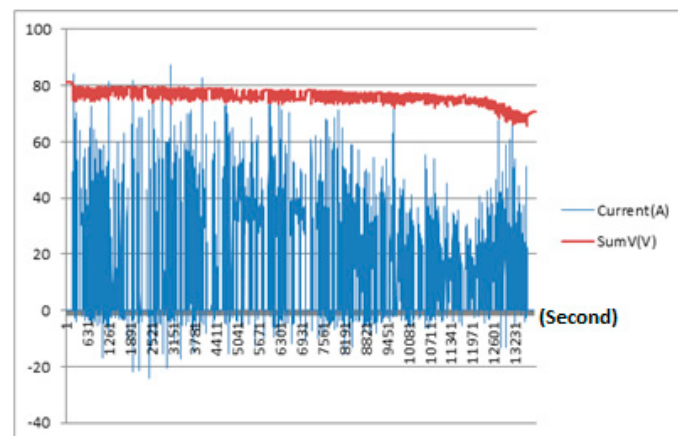


Figure 11. Histories of battery voltage and current.

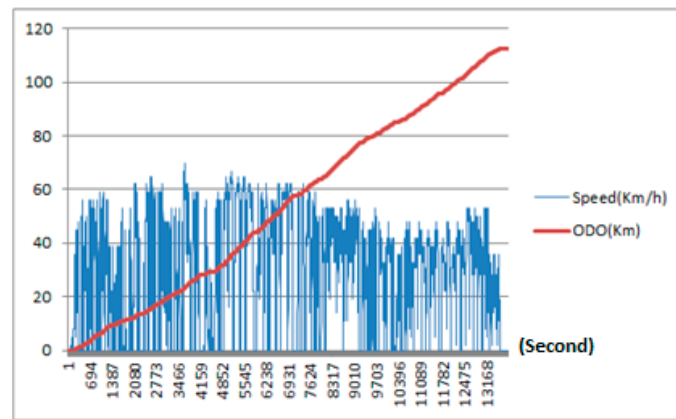


Figure 12. Histories of vehicle speed and accumulated mileages (ODO).

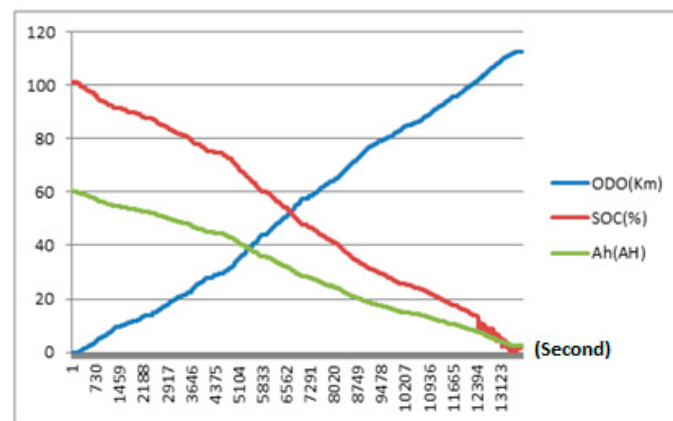


Figure 13. Histories of accumulated mileages, SOC and accumulated Ah.

3.3. Range Extension Benefits of Two-Stage Charging and Balancing Method

The second stage of the developed method can fully charge every cell and could have range extension benefits. Charging tests with the second stage and without the second stage are conducted, respectively, discharging with the same 72 V e-motorcycle platform. Test results are summarized in Table 2, where the first two tests charge the main battery without the second stage and the battery only accepts 45.1 Ah and 43.7 Ah, both close to 70% of the battery’s full capacity. The driving ranges for these two cases are 86.4 kM and 85.59 kM, respectively.

Table 2. Discharging results for three sets of conditions.

Mode	Charging Strategy	Accumulated Ah	Mileage	Cell Voltage Difference after Discharging
Charging	Charging in Series	45.1 Ah	-	25 mV
Discharging	-	43.4 Ah	86.4 Km	438 mV
Charging	Charging in Series	43.7 Ah	-	22 mV
Discharging	-	42.1 Ah	85.59 Km	546 mV
Charging	Charging in Series + Cell Charging one by one	60 Ah	-	23 mV
Discharging	-	57.9 Ah	114.2 Km	448 mV

The third test in Table 2 adopts second stage charging and 60 Ah is injected into the main battery. The driving range of this case is 114.2 kM and 57.9 Ah is discharged before the low voltage is reached. Close to 28 kM of driving range is gained if the complete two-staged charging is implemented. In other words, the developed two staged charging method has range extension benefits.

It is noticed in the first two tests of Table 2 that the cell voltage inconsistency or difference deteriorated if the second stage of charging is not implemented. If the second stage of charging is implemented, the cell voltage inconsistency could be improved as shown in the third case of Table 2. Since cell voltage inconsistency greatly affects battery efficiency, two staged charging is therefore capable of enhancing battery efficiency by reducing voltage inconsistency.

4. Conclusions

This study successfully builds a 72 V BMS by separating a globally active balance module from the BMS. The remaining BMS or main control subsystem is electrically connected with the main battery module inside a 72 V motorcycle to measure cell operation parameters, protect cells from extreme operation limits, and extract and monitor vehicle power parameters. An independent globally active balance module is placed on the charger side. Without the limitation of restricted space in the battery module, the separate balance module can balance cells with large balance currents to accelerate the balance speed since heat dissipation is easy to implement outside the battery module. A two stage charging method based on the globally active balance circuit is shown to charge every cell in series connection to its full state without suffering any degree of overcharging. Range extension benefits of the two stage charging method are also verified in test drives. Cell inconsistency-related efficiency problems are alleviated greatly with the developed independent globally active balance module.

Acknowledgments: The author would like to gratefully acknowledge the supports from Taiwan Ministry of Science and Technology under the contract numbers: NSC102-2622-E-167-012-CC3 and MOST103-2622-E-167-009-CC3.

Conflicts of Interest: The current author declares no conflict of interest.

References

1. Lu, L.; Han, X.; Li, J.; Hua, J.; Ouyang, M. A review on the key issues for lithium-ion battery management in electric vehicles. *J. Power Sources* **2013**, *226*, 272–288. [[CrossRef](#)]
2. Rahimi-Eichi, H.; Ojha, U.; Baronti, F.; Chow, M. Battery management system: An overview of its application in the smart grid and electric vehicles. *IEEE Ind. Electron. Mag.* **2013**, *7*, 4–16. [[CrossRef](#)]
3. Aizpuru, I.; Iraola, U.; Canales, J.M.; Echeverria, M.; Gil, I. Passive balancing design for Li-ion Battery Packs based on single cell experimental tests for a CCCV charging mode. In Proceedings of the International Conference on Clean Electrical Power, Alghero, Italy, 11–13 June 2013; pp. 93–98.
4. Laka, A.; Barrera, J.A.; Chivite-Zabalza, J.; Rodríguez, M.Á. Passive Balancing of the DC Bus Midpoint for Neutral Point Clamped (NPC) Based Voltage Source Converters. *IEEE Ind. Electron. Soc.* **2013**, 1148–1153. [[CrossRef](#)]
5. Cao, J.; Schofield, N.; Emadi, A. Battery balancing methods: A comprehensive review. In Proceedings of the Vehicle Power and Propulsion Conference, Harbin, China, 3–5 September 2008; pp. 1–6.
6. Zheng, Y.; Ouyang, M.; Lu, L.; Li, J.; Han, X.; Xu, L. On-line equalization for lithium-ion battery packs based on charging cell voltages: Part 1. Equalization based on remaining charging. *J. Power Sources* **2014**, *247*, 676–686. [[CrossRef](#)]
7. Gallardo-Lozano, J.; Romero-Cadaval, M.; Milanés-Montero, M.; Guerrero-Martinez, M. Battery equalization active methods. *J. Power Sources* **2014**, *246*, 934–949. [[CrossRef](#)]
8. Baronti, F.; Roncella, R.; Saletti, R. Performance comparison of active balancing techniques for lithium-ion batteries. *J. Power Sources* **2014**, *267*, 603–609. [[CrossRef](#)]
9. Moran, J. *PowerPump™ Balancing*; Texas Instruments Application Report, SLUA524A; Texas Instruments: Dallas, TX, USA, 2011; pp. 1–15.
10. Lin, J.C.M. Development of an global and active balance circuit. *J. Soc. Nav. Arch. Mar. Eng.* **2012**, *31*, 53–59.
11. DANUBE, Inc. FEWS-4804.5B30 Datasheet, FEWS-6004.5B30 Datasheet. Available online: <http://www.powerdatasheet.com/uploadfiles/Files/PDF/2233/20150323152209366.pdf> (accessed on 3 June 2017).
12. NXP Semiconductors N.V. BUK956R1-100E Datasheet. Available online: <http://www.datasheets360.com/pdf/-689899174041966393> (accessed on 5 June 2017).

13. Microchip Inc. PIC18F87K22 Datasheet. Available online: <http://www.microchip.com/wwwproducts/Devices.aspx?dDocName=en546891> (accessed on 2 May 2017).
14. Letex Technology Corp. LT210 Datasheet. Available online: http://www.letex.com.tw/products_detail.php?cate=57 (accessed on 3 April 2017).
15. Lin, J.C.M. Study of Lithium Ion Cell Voltage Measuring Circuits. *J. Technol.* **2012**, *15*, 1–10.
16. Allegro, Inc. ACS756 Datasheet. Available online: <http://www.allegromicro.com/~media/Files/Datasheets/ACS756-Datasheet.ashx> (accessed on 12 June 2017).
17. Winson Semiconductor Corp. WSH132 Datasheet. Available online: <http://www.alldatasheet.com/datasheet-pdf/pdf/714671/WINSON/WSH132.html> (accessed on 25 May 2017).
18. Analog Devices, Inc. ADM2687E Datasheet. Available online: http://www.analog.com/static/imported-files/data_sheets/ADM2682E_2687E.pdf (accessed on 18 May 2017).
19. Letex Technology Corp. LT218 Datasheet. Available online: http://www.letex.com.tw/products_detail.php?cate=57 (accessed on 3 April 2017).



© 2017 by the author. Licensee MDPI, Basel, Switzerland. This article is an open access article distributed under the terms and conditions of the Creative Commons Attribution (CC BY) license (<http://creativecommons.org/licenses/by/4.0/>).